JOURNAL OF CATALYSIS 144, 60–76 (1993)

Rapid Sintering in NO of Nanometre-Sized Pt Particles on γ-Al_2O_3 Observed by CO Temperature-Programmed Desorption and Transmission Electron Microscopy

P. LÖÖF,* B. STENBOM,†[1] H. NORDÉN,† AND B. KASEMO*

*Department of Applied Physics and †Department of Physics, Chalmers University of Technology, S-412 96 Göteborg, Sweden

Received October 30, 1992; revised February 26, 1993

The dispersion loss due to sintering of nanometre-sized Pt particles on porous γ-Al_2O_3 was measured in different atmospheres (Ar, H_2, O_2, CO, NO) at temperatures 200–700°C. The methods used were temperature-programmed desorption with CO as the dispersion probing molecule, and transmission electron microscopy, respectively. The sintering rate was negligible in Ar and H_2, accelerated in O_2, as reported by several previous investigators, and dramatically enhanced in NO compared to O_2. Possible sintering mechanisms are discussed.

1. INTRODUCTION

The efficiency and life-time of a supported metal catalyst is influenced by the stability of the highly dispersed metal particles. The sintering (particle coarsening) rate depends on the operating temperature, time, and chemical environment (reducing, oxidizing, inert, etc.). A large number of studies have investigated the phenomenon of sintering (*1–23*). In several of these studies the sintering of Pt/Al_2O_3 catalysts was observed to be more pronounced in O_2 than in H_2 (above 600°C) (*3, 7, 9, 10*). Redispersion of Pt/Al_2O_3 catalysts during exposure to oxygen at 500–600°C was also reported (*5, 10, 12, 16*). Two types of mechanism were proposed to explain the observed sintering behaviour. The atomic migration model (*14–16*) involves the transport of individual atoms between particles, whilst the particle migration model (*17, 18*), includes the migration of whole particles over the support, followed by collision and coalescence. In the particular case of automotive catalysts, growth of the precious metal particles leads to larger emissions during warm-up due to an increased light-off temperature (*23*).

In this work we have investigated the sintering of alumina-supported platinum catalysts exposed to different atmospheres (H_2, O_2, CO, NO) and reaction conditions at elevated temperatures. The methods used to follow changes in the platinum metal dispersion, were thermal desorption "spectroscopy" of carbon monoxide (CO-TDS) and transmission electron microscopy (TEM). A remarkably high sintering rate was observed with NO.

2. EXPERIMENTAL

2.1. Samples

The catalysts were prepared by coating a monolithic support of cordierite (cylindrical 30 × 22 mm, 62 cells/cm^2) with γ-alumina. The alumina (Condea PX140, 140 m^2/g BET area) was ground in a ball mill together with an aqueous solution of H_2PtCl_6 before the alumina was applied to the monolith. This was made to ensure an even distribution of 1 wt% platinum throughout the washcoat.

All samples were dried in air and reduced in 4% H_2/N_2 for 2 h at 500°C prior

[1] To whom correspondence should be addressed.

0021-9517/93 $5.00

to experiments. The preparation of the catalysts was made by Svenska Emissionsteknik AB.

Samples used for the sintering and TDS measurements were cut out as blocks of 6 × 6 channels (8 × 8 mm) of about 14 mm length to fit in the quartz flow reactor. The sample weight was 0.5–0.6 g. A minor loss of the Al_2O_3 washcoat was observed with some samples as a result of the cutting.

2.2. *Experimental Systems and Procedures*

TDS. The sintering of the catalysts and the CO-TDS (thermal desorption spectroscopy with carbon monoxide) measurements were performed at atmospheric pressure in a quartz flow reactor (*24*), on-line connected to a quadrupole mass spectrometer. The composition of the effluent gas flow was continuously analyzed by the mass spectrometer via a quartz capillary probe (*25*) positioned at the centre axis, about 10 mm downstream from the catalyst sample. A carrier gas of argon (30 ml/min) continuously flowed through the reaction cell during the TDS experiments. Linear temperature-versus-time heating of the reaction cell and sample up to 1000°C was obtained with an external heating coil. The temperature of the sample was measured by a 0.3-mm-diameter, chromel–alumel thermocouple located in one of the channels of the catalyst.

The entire flow system, consisting of the reaction cell and gas handling system, was initially evacuated down to 10^{-3} Pa, and helium leak-tested in order to guarantee a leak-free system. The connections to the reaction cell were, after every change of sample, helium leak-tested to ensure that no leaks were introduced. The effect of a leak was immediately observed as a higher than normal CO_2 signal during the TPD runs due to catalytic oxidation of CO. The daily start-up procedure was always to evacuate the entire flow system down to 10 Pa before the gas flows were switched on. The purpose was to avoid high levels of initial impurities in the gas flows and contamination of the gas supplies.

Quantitative measurements of desorbing CO and CO_2 were obtained by calibrating the mass spectrometer using known gas mixtures and the known flow rate of the carrier gas. The gas mixtures (used without further purification) were ultra high purity 4% H_2 in Ar, 4% CO in Ar, 4% and 0.1% NO in Ar, 2% O_2 in Ar, and 100% Ar, respectively (99.9997% purity, delivered from Alfax). Initially the samples were found to be contaminated with nickel when the ageing was performed in CO + O_2, CO + NO, and CO at elevated temperatures. The source was found to be trace amounts of nickel carbonyls in the CO + Ar mixture, which thermally decomposed on the samples. The deposition of nickel on the samples was successfully avoided using a trap consisting of a heated tube filled with quartz wool.

TDS measurements were conducted with samples subjected to the following pretreatment procedure. First the sample was reduced in 4% H_2 in Ar at 600°C for 10 min. This temperature was found to be an optimum choice in order to avoid thermal sintering at higher temperatures and incomplete reduction at lower temperatures. (Samples reduced at temperatures below 600°C were incompletely reduced as shown by a higher CO_2 signal in the CO-TDS spectra.) The reaction cell was then flushed with Ar for 1 min and cooled to room temperature over a period of 7 min.

The TDS experiments were initiated by exposing the samples to 4% CO in Ar for 1 min. After the CO had been switched off and the CO signal had reached the background level, i.e., no gas-phase CO present, TDS runs were performed by heating the reaction cell at a rate of 2 K/s to 600°C. CO and CO_2 were continuously analyzed by the mass spectrometer during the TDS run. From the integrated amount of CO desorption in such runs, a measure of the dispersion of the fresh sample was obtained.

The experiment to explore sintering deactivation of a sample was performed immediately after a TDS run as described above,

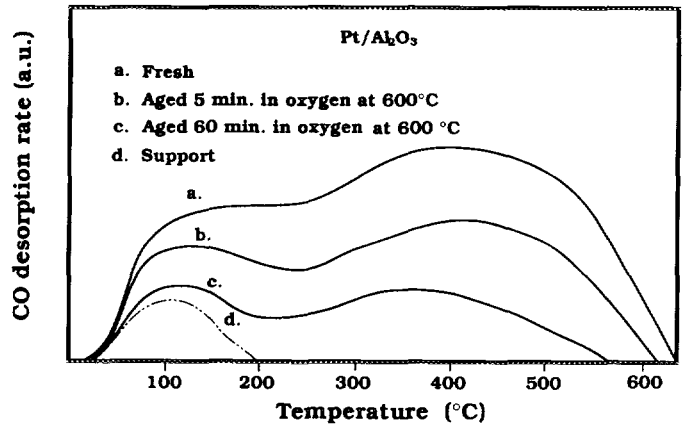

FIG. 1. TDS spectra of CO after CO adsorption at room temperature on reduced catalysts. (a) fresh sample, (b) and (c) aged 5 and 60 min, respectively, in oxygen at 600°C, and (d) Al_2O_3 support.

by increasing or decreasing the sample temperature to the selected sintering temperature and then injecting a flow of the selected gas. The sintering was interrupted at regular time intervals in order to measure the dispersion change by CO-TDS. The procedure was completed with a final dispersion measurement, which includes reduction in H_2, before the sample was taken out and investigated by TEM.

When the dispersion was calculated the measured amount of desorbed CO (about 0.2 μmol; see Fig. 1) from a blank sample of Al_2O_3 was subtracted from the measured, integrated CO-TDS signal. The CO-TDS signal from the blank support was found to be unaffected by high-temperature treatment in O_2, 700°C/30 min, or NO, 500°C/30 min.

TEM analysis. TEM specimens were prepared by the conventional crushed powder technique described by, for example, Rice and Treacy (*26*). Parts of the washcoat layer were abraded away and crushed with a mortar and pestle. The powder was ultrasonically dispersed in methanol and transferred onto a holey carbon film, supported on a copper grid.

Transmission electron microscopy was performed using a JEOL 2000 FX TEM/STEM to determine particle size distribution and washcoat composition. The microscope is equipped with a LINK, X-ray energy dispersive spectrometer (EDS). Micrographs at high magnification (normally ≈400,000) were recorded from the catalyst samples. Particle size measurements were made on the negatives.

Electron microscopy of supported catalysts is *in principle* a quite straightforward method to determine the particle size distribution, but as mentioned earlier by Flynn *et al.* (*27*) and Treacy and Howie (*28*) there are in reality several limitations and assumptions involved.

Ideally it should be possible from the particle size distribution to calculate the metal dispersion, D = ratio of the number of surface atoms to the total number of atoms. By applying a simple model using a spherical particle geometry as discussed, for example, by Freel (*13*), one obtains

$$D = \frac{6v}{s}\left(\sum_1^N d_i^2 \Big/ \sum_1^N d_i^3\right), \qquad (1)$$

where d_i is the diameter of the ith particle, s is the area occupied by one metal atom at the surface ($s \approx 8.4$ Å^2 as an average for the (100), (110), and (111) planes was used), v is the volume occupied by one metal atom in the bulk ($v \approx 15.1$ Å^3 for platinum), and

N is the number of particles in the set of particles used to determine D. Note that the same expression as above is obtained if we assume half spheres, with the flat area in contact with the support. We use this model in the analysis below, but must then also point out some important limitations and reservations.

Particle shapes may certainly deviate from spherical and, in addition, take different forms at different sizes. For example, the particle shape and surface area are influenced by the strength of the metal–support interaction and by the tendency to form crystalline facets. Furthermore, to obtain the dispersion D from the measurements and Eq. (1), a representative and sufficiently large number of particles must be measured, which is very time-consuming and sometimes impossible. Especially when the average particle size is small, the smallest ones may not be registered at all and give rise to a systematic error. There are also sometimes problems to ascertain that the measured d_i from micrographs are corresponding to the true particle sizes.

With these reservations in mind we still find it meaningful and even illustrative to apply Eq. (1) in order to make a semiquantitative comparison possible between CO-TDS and TEM-estimates of the dispersion values. For the reasons given above we emphasize the overall trends and the comparisons between results with different gases, and TDS–TEM comparisons, respectively, rather than absolute numbers.

3. RESULTS

3.1. *Fresh Samples*

Figure 1, curve (a), shows a representative CO-TDS spectrum obtained from a fresh sample. It consists basically of two broad contributions centered around 100 and 400°C. The TDS spectrum is in agreement with the spectra observed by Foger and Anderson (*29*) and by Herz and McCready (*30*) from Pt/Al_2O_3 samples with dispersions of 40%, containing 0.9 and 1 wt% Pt, respectively. In all CO-TDS runs there was also a small CO_2 signal in the temperature range 250–500°C, whose integrated magnitude was less than 10% of the CO signal. The CO_2 peak was in a former study (*31*) associated with trace amounts of oxygen in the feed gases. The total amount of desorbed CO during a TDS run is obtained from the area under the TDS curve, since the gas flow rate is known and the CO concentration is measured quantitatively. The dispersion is then calculated using the known amount of Pt in the samples and assuming an adsorption stoichiometry of 0.7 CO molecules per Pt surface atom. The chosen CO/surface Pt ratio is close to the value observed for many CO–metal single crystal systems including Pt (*32*) but may be debated. A range of values has been reported (*33–38*), for example about 0.9 for Pt particles less than 5 nm and about 0.5 for larger particles, (Pt dispersions$<$ 20%) (*35*). The calculated dispersion from our CO-TPD measurements of the fresh samples was in the range 36–50%. The uncertainty in adsorption stoichiometry prevents a quantitative analysis of the dispersion results.

TEM micrographs of fresh samples showed regions with varying density of very small, $\leq$1 nm, hardly visible platinum particles (Fig. 2 a). The variation in initial dispersion values, measured with CO-TDS, may be caused by different particle sizes in the fresh samples, i.e., by an inherent spread in the preparation procedure, and/or by the abovementioned (Section 2.1) loss of Al_2O_3 washcoat during cutting. TEM micrographs of different fresh samples support at least partly the latter explanation since they show particles with approximately the same sizes $\leq$1 nm, (e.g., with a low initial dispersion of 36% one should have detected particles with sizes $\geq$1.5 nm).

3.2. *Reducing and Inert Atmospheres (Ar, H_2, and CO)*

Ar and H_2. Exposing the catalyst sample to an inert atmosphere of pure argon at 700°C for 60 min produced no change in the CO-TDS spectra. The stability of the

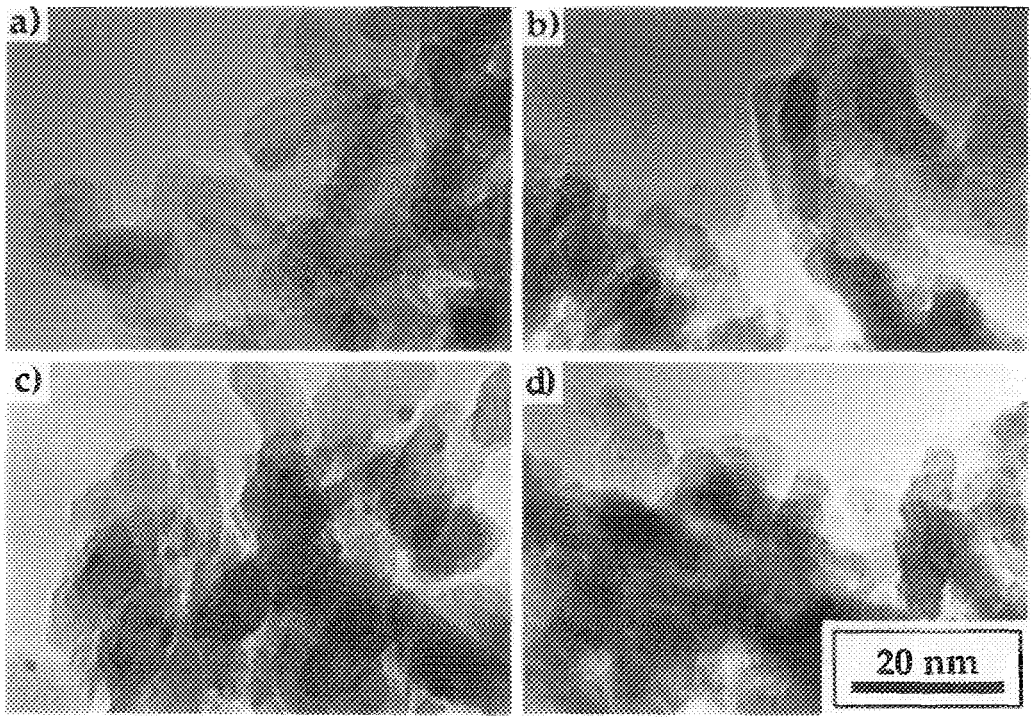

FIG. 2. TEM micrographs of catalysts showing the alumina washcoat with only small platinum particles: (a) fresh, (b) 4% H_2 in Ar, 700°C/60 min; (c) 4% CO in Ar, 600°C/65 min; and (d) 2% O_2 in Ar, 500°C/60 min.

catalyst in the inert atmosphere at 700°C was confirmed by TEM measurements since TEM micrographs were identical to the ones for fresh samples.

Also with H_2 no decrease in dispersion was observed on a sample exposed to 4% H_2 in Ar at 600°C for 60 min. (This result made it possible to reduce all samples for 10 min at this temperature prior to all CO-TDS measurements.)

Raising the temperature to 700°C and 60 min exposure leads to a minor drop in dispersion (Fig. 3) as obtained from CO-TDS. This decrease in dispersion was too small to be distinguished in TEM micrographs (Fig. 2b).

CO. Two samples were heated in 4% CO in Ar at different temperatures. No change in dispersion was detected by CO-TDS when the first sample was exposed to CO at 250°C for 180 min. Subsequent heating in CO at 410°C for 80 min resulted in a change in the TDS spectrum towards higher CO desorption temperatures. It was then necessary to increase the temperature to 700°C in order to remove all CO. Subseqeunt reduction in H_2 in Ar at 600°C for 10 min followed by a second TDS-run resulted in a normal CO desorption spectrum with no detected decrease in dispersion. TEM micrographs confirmed this, as the particles had the same sizes as in fresh samples.

The second sample was exposed to CO at 600°C for 65 min, which increased the particle size to $\approx$1.8 nm in TEM micrographs (Fig. 2c) and reduced the dispersion obtained from CO-TDS from 46 to 32%. This sample exhibited a normal CO desorption spectrum directly after CO exposure. The CO-induced change in the desorption spectrum for the sample heated at 410°C is tentatively attributed to carbon deposition on Pt

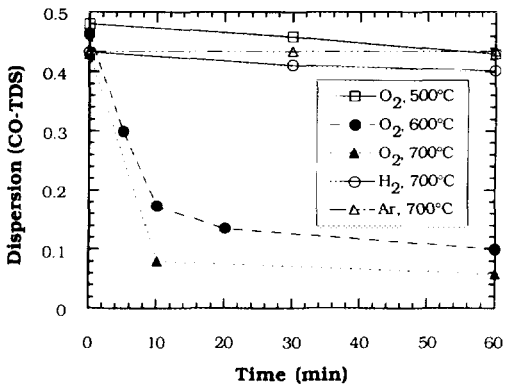

FIG. 3. The decrease in dispersion versus time at different temperatures for samples exposed to oxygen. For comparison, curves representing sintering in hydrogen and argon at 700°C are also shown.

via the reaction CO + CO → CO_2 + C or CO-induced faceting of Pt surfaces. In summary, the effects of CO on the dispersion are small over the studied temperature range.

3.3. *Oxidizing Atmospheres*

O_2. Catalyst samples were exposed to a 300 ml/min gas flow of 2% O_2 in Ar at 500°C, 600°C and 700°C for 60 min. The change in dispersion was tested at regular intervals by CO-TDS runs. Figure 1 shows the TDS curves obtained from the sample aged at 600°C for 5 and 60 min (curves (b) and (c), respectively). The figure also shows the TDS curves from the fresh sample (a) and the support (d). These curves clearly demonstrate a loss of Pt surface area, i.e., of dispersion. They also show that the relative amount of CO desorption loss in the 100°C peak is considerably larger than in the high-temperature peak. In curve (c) there is almost no desorption at 100°C, when corrected for the desorption from the support (dotted curve (d)). The decreases in dispersion due to oxygen exposure at 500, 600, and 700°C, extracted from these TDS runs, are shown in Fig. 3. For comparison, curves representing sintering in hydrogen and argon at 700°C are shown. It is clearly seen that the sintering is much faster in the presence of oxygen than in H_2 or Ar.

The dispersion decrease in O_2 at 500°C is, however, quite moderate, indicating that the catalyst is nearly stable towards oxygen at this temperature. TEM measurements confirmed this mild ageing, since the particles have about the same size (≈1 nm) as in the fresh samples (Fig. 2d).

When the ageing temperature was increased to 600 and 700°C a fast increase in sintering rate was observed; 60-min ageing at these temperatures resulted in dispersion values of only 10 and 6% respectively, i.e., a decrease in surface area by a factor of 4 and 8, respectively. The initial sintering rate over the first 10 min is fast and then decays towards almost constant Pt area after 60 min. TEM micrographs confirm these ageing kinetics and show platinum particles in the size range 2–10 nm for the 600°C/60 min sample and in the range 2–11 nm for the 700°C/60 min sample. Figure 4 show micrographs of the 700°C sample.

In order to determine the absolute oxygen content in the platinum particles, oxidation in O_2 at 500°C was performed, followed by first flushing with Ar and then reducing in CO at the same temperature. The integrated CO_2 production during the reduction corresponds to an O/Pt ratio of about 1.5 which indicates bulk oxidation of the Pt particles during the O_2 exposure. (See Ref. (*24*) for details about quantification of reduction–oxidation runs like this one).

To further elucidate the role of oxygen in the sintering, two additional experiments were performed. In the first experiment a reduced catalyst, mildly sintered to 25% dispersion, was exposed to a gas flow of 2% O_2 in Ar at room temperature. At this low temperature primarily chemisorption, and little or no bulk oxidation, is expected. With 25% dispersion and assuming a maximum chemisorption layer density of one oxygen atom per two Pt atoms (*32*), the average O/Pt ratio will be 1/8. The sample was then flushed with Ar until the oxygen signal had reached the background level (no gas phase

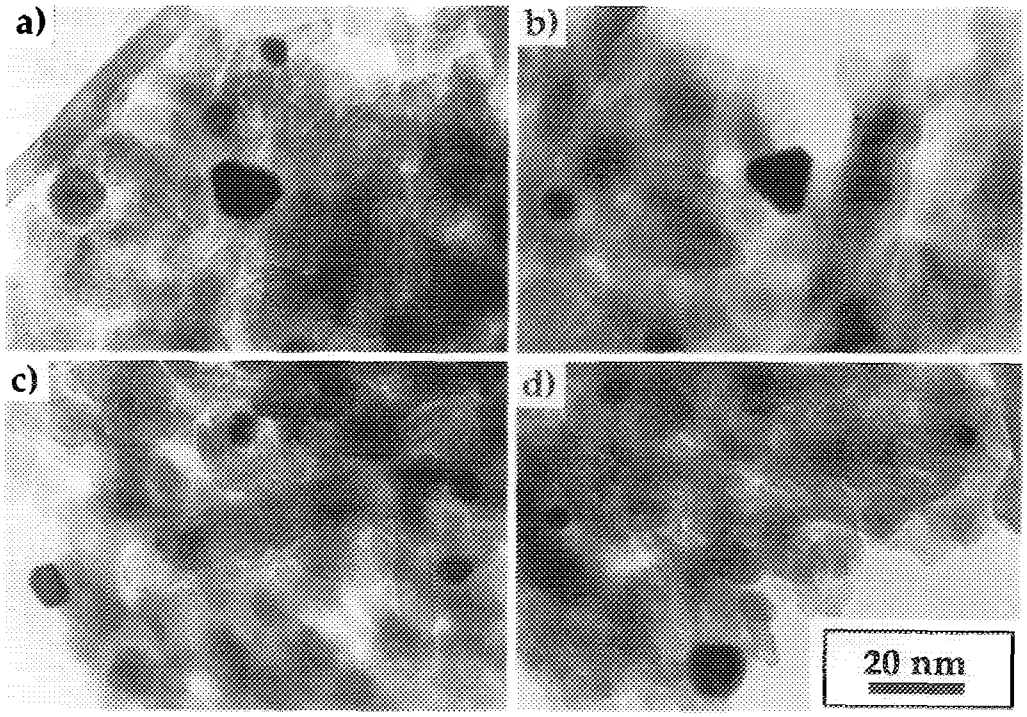

FIG. 4. TEM micrographs of catalyst aged in 2% O_2/Ar at 700°C for 60 min showing large sintered Pt particles.

O_2 present), heated linearly to 700°C, and held at this temperature for 10 min. During this treatment no oxygen desorbed, as shown by the absence of an oxygen signal in the mass spectrometer. A small decrease in dispersion to 23% was observed by CO-TDS.

The second experiment was performed by oxidizing the same sample at 500°C for 10 min (after the run described above). The sample was then cooled to room temperature and the same experimental sequence as above was repeated. During the heating of the sample in Ar, a small amount of oxygen desorbed around 500°C. The amount corresponded to about 0.1 oxygen atom per Pt atom. For this preoxidized sample, which contained considerably more oxygen than in the first experiment, a significant decrease in the dispersion from 23 to 11% was observed by CO-TDS. These two experiments indicate that bulk oxidation is necessary for the accelerated sintering in O_2, while Pt particles with only chemisorbed oxygen are much more stable.

NO. Samples were exposed to a gas flow of 300 ml/min of 0.1% NO in Ar at 200°C (10, 25, and 160 min), 300°C (10, 30, 60, and 120 min), and 500°C (10, 30, and 60 min), and to 4% NO in Ar at 300°C (10, 30, and 60 min) and 500°C (10 and 20 min). The sintering rate in NO was, surprisingly, much higher than that for samples exposed to oxygen, as seen in Fig. 5. For example, the sintering rate in NO is already at 200°C more pronounced than in O_2 at 500°C. As with oxygen, the sintering rate is increasing with temperature, and the initial rate is fast and then decays monotonically with time. The same relatively larger decrease in the CO desorption peak at low temperatures, as with O_2, was observed.

Figure 5 also shows that at 300 and 500°C the sintering rate is somewhat faster for the

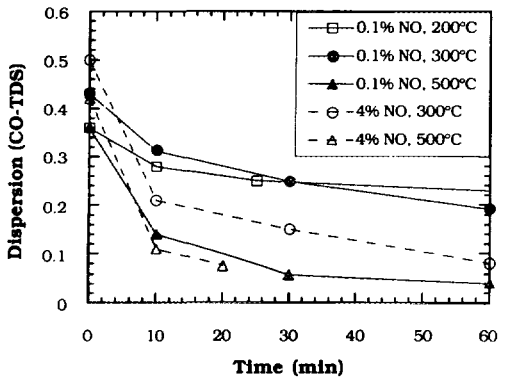

FIG. 5. The decrease in dispersion versus time at different temperatures for samples exposed to 4% and 0.1% NO in Ar.

samples exposed to 4% NO in Ar compared to the samples exposed to 0.1% NO in Ar.

The dispersion values after ageing in 0.1% NO in Ar decreased to 17, 15, and 4% for the 200, 300, and 500°C samples, respectively. TEM micrographs of these samples show particles in the range of 2–5, 2–8, and 5–14 nm, respectively. Figure 6 show micrographs of the 500°C sample. Thus the severe sintering in NO observed by CO-TDS is confirmed by and consistent with the TEM results. The shape of the sintered Pt particles appeared to be independent of whether NO or O_2 was used.

The difference between the sintering effects by oxygen and NO could possibly be due to a higher oxygen content deposited on the Pt particles by NO than by O_2. This idea was tested with oxidation/reduction runs at 500°C, performed in the same way as in the case of O_2 but now with NO as the oxidant. The same amount of CO_2 was produced after oxidation, indicating that the oxygen amount deposited was the same with NO as with O_2.

Another possibility to consider is that the observed sintering in NO is reaction enhanced (e.g., by the NO dissociation and/or N_2 recombination reactions $2NO + 2Pt \rightarrow N_2 + 2PtO$). This hypothesis was tested by monitoring the sintering rate and reaction products formed during NO exposures of an oxidized (O_2, 5 min, 500°C) sample and a reduced (H_2, 10 min, 600°C) sample, respectively. The samples were exposed to 300 ml/min of 0.1% NO in Ar at 500°C for 10 min and the mass spectrometer was monitoring masses 30 (NO), 32 (O_2), 28 (CO or N_2), 44 (CO_2 or N_2O), and 46 (NO_2). The only reaction product detected from the prereduced sample was N_2. No reaction products were detected from the preoxidized sample. Reactions may occur at undetectable small reaction rates or with no net products (e.g., the sequence: NO-adsorption – dissociation – recombination – desorption). More likely, however, is the earlier reported oxygen poisoning of the NO dissociation (*31*). No marked difference in the sintering rate was observed between the reduced and oxidized samples. Thus no evidence was found supporting the hypothesis that the sintering was reaction driven.

A more conclusive way to exclude the possibility of a reaction-induced sintering was to age the sample by conducting TDS runs with NO. This procedure gives a better control over the amount of oxygen deposited on the catalyst and minimizes the presence of gas-phase NO. NO-TDS runs were performed in a similar way as described in the experimental section for CO-TDS runs. NO was adsorbed on the sample by injection of a 50 ml/min flow of 0.1% NO in Ar into the carrier gas for 10 s. In these NO-TDS runs the sample was not heated above 480°C in order to avoid sintering caused by the oxygen content in the Pt particles. Four such experiments, each involving a series of six TDS runs with NO, were performed in slightly different ways in order to elucidate the observed sintering in NO. The dispersions of the samples used in these experiments were measured by CO-TDS before and after each experiment. The six NO-TDS runs in the first experiment were all performed on fully reduced samples (i.e., with reduction in H_2 between each run). Only N_2 was detected. No sintering was observed after this experiment. In the second experiment, reduction was only performed after

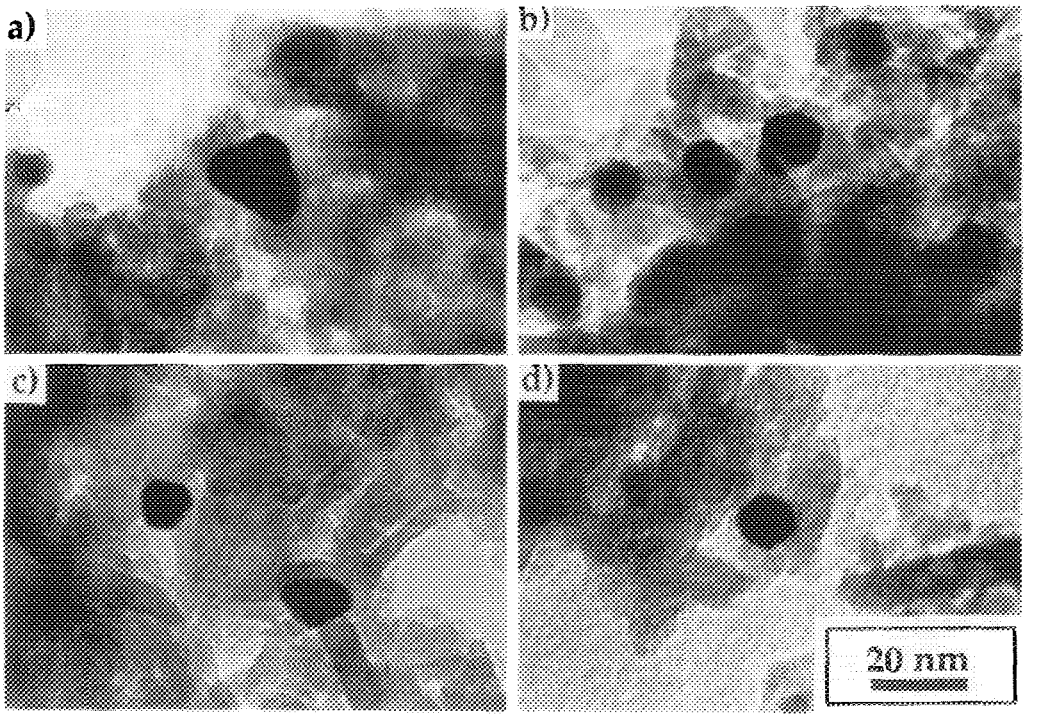

FIG. 6. TEM micrographs of catalyst aged in 0.1% NO/Ar at 500°C for 60 min showing large sintered Pt particles.

every two NO-TDS runs. A small amount of NO was detected during the second of the two successive TDS runs. No change in dispersion could be measured in this case either. In the third experiment all six successive NO-TDS runs were performed, without reduction between the runs. This resulted in a decline in the N_2 signal, and a concerted rise in the NO signal after each run, as observed in an earlier study (*31*). A small but significant decrease in dispersion was observed in the CO-TDS measurements performed after this experiment. The last TDS experiment was performed exactly as the third but the TDS runs were performed with a sample that prior to the first NO exposure was oxidized in O_2 at 480°C for 5 min. Only NO was found to desorb from this sample during the six TDS runs. This sample showed a clear decrease in dispersion (a relative reduction of about 20%), which is larger than in any of the three previous experiments. These series of experiments clearly show that it is molecular *NO adsorbed on oxidized Pt particles* that is responsible for the high sintering rate in NO.

Exactly the same behaviour was observed when one reduced (H_2, 600°C, 10 min) and one oxidized (O_2, 480°C, 5 min) sample were exposed to a small gas flow of 7 ml/min of 0.1% NO in Ar at 500°C for 8 min. For this NO dose the reduced sample converted all NO to N_2 in contrast to the oxidized sample which did not produce any N_2 during the exposure to NO. The decrease in dispersion was significantly higher for the oxidized sample, which indicated, as the TDS experiments above, that the sintering process in NO must be associated with molecular NO adsorbed on oxidized Pt particles.

3.4. Gas Mixtures

CO + O_2. Samples were fed with an equal flow of 2% O_2 and 4% CO in argon. The

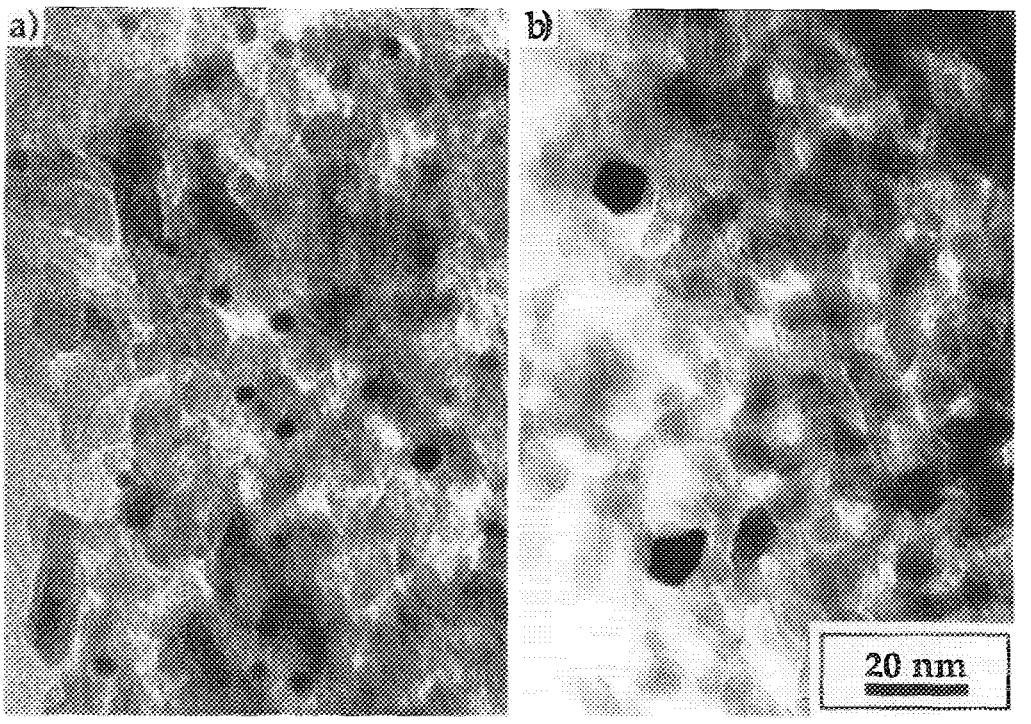

FIG. 7. TEM micrographs of catalyst (a) aged in CO + NO/Ar at ≈475°C for 8 min showing Pt particles in the range 1–5 nm and (b) aged in 4% NO/Ar at 500°C for 10 min showing much larger sintered Pt particles compared to those in (a).

temperatures were chosen to give 50% conversion of the reactants at different flows to assure that the whole length of the catalyst was participating in the oxidation of CO to CO_2. No sign of sintering was observed by CO-TDS at 250°C/120 min, 320°C/30 min, and 370°C/22 min. TEM micrographs show only particles with the same sizes as seen in the fresh samples. The reaction heat generated by the exothermic reaction thus does not induce sintering at these temperatures.

CO + NO. Feeding the catalyst with equal flows of 2000 ml/min of 4% CO and 4% NO in argon at around 400°C for 5 min with subsequent ageing at 475–500°C (≈50% conversion) for 8 min resulted in Pt particles in the range 1–5 nm (Fig. 7a) and a resulting dispersion of 15% (from CO-TDS). Ageing a catalyst with NO alone at 500°C for 10 min resulted in a dispersion of 6% from CO-TDS and TEM micrographs then show Pt particles between 5–12 nm (Fig. 7b). Thus the sintering in NO alone is higher than in CO + NO and again no indication of a reaction enhanced sintering was observed.

4. DISCUSSION

The most important result of this study is the surprising acceleration of the particle sintering rate in NO compared to O_2, which was observed both with CO-TDS and TEM. Another interesting observation was the change in the TDS spectra as the particle size increases. We first discuss the last observation and the estimation of dispersion values from the CO-TDS and TEM results.

CO-TDS Spectra

A general trend during ageing is that the amount of CO desorption around 100°C decreases, in relative magnitude, more than the CO desorption at higher temperatures.

Eventually the low-temperature desorption completely vanishes for samples with dispersion values below 5% (CO-TDS). According to Rothschild and Yao (*38*), this is indicative of special metal–support interaction in the small particles. TEM micrographs of the low dispersed samples did not show Pt particles with sizes <2 nm. The low-temperature peak can therefore be associated with CO desorption from Pt particles less than about 2 nm in size. A similar observation and conclusion was earlier reported by Herz and McCready (*30*), who observed a decrease in the low-temperature peak by about 50% when the dispersion at the same time dropped from 100 to 70% on a highly dispersed Pt/Al_2O_3 catalyst. They also associated the low-temperature peak with CO desorption from very small Pt particles (<1.1 nm). Thus the result of sintering is not only a decrease in surface area, but it also changes the character of the binding sites for CO. It is likely that the CO binding site, corresponding to the low-temperature peak (i.e., small particles <2 nm), has a different CO/Pt stoichiometry than the stoichiometry on large bulk like particles. (For a discussion, see Refs. (*35–37*).)

Comparison between TDS and TEM Dispersion Values

From the preceding discussion it is apparent that a precise determination of the metal dispersion of supported catalysts, measured by CO-TDS or TEM, is difficult. In both cases certain assumptions are required to obtain absolute numbers. For TDS the chemisorption ratio CO/Pt on the surface is needed and the dependence of the CO/Pt ratio on particle size is not well known. In TEM micrographs the two-dimensional projection of the particles is recorded while the three-dimensional structure, necessary to calculate dispersion, is difficult to obtain. Particles are normally not spherical or half-spherical as assumed in our model to calculate the dispersion (from TEM data). Furthermore the contact surface area between particles and support is unknown and not

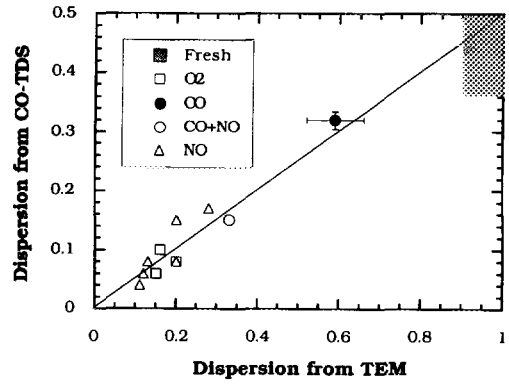

FIG. 8. Comparison between dispersion values calculated from TEM and CO-TDS results. The large spread in fresh samples is represented by the shaded area. The straight line is drawn to help the eye.

expected to be a constant fraction of the total surface area for different particle sizes. Finally, very small particles (<1 nm) are not distinguished in the TEM micrographs. However, if we accept the assignment of the 100°C CO-TDS peak to originate from very small particles, the latter problem is not so severe except at high dispersion values.

In spite of these uncertainties it is still of interest to explore the relation between the TDS and TEM dispersion measurements, using the CO-TDS and TEM data compiled in Table 1. The correlation in Fig. 8 is, considering the involved approximations (Eq. (1)) and the other uncertainties mentioned above, fairly good (the straight line is drawn to help the eye). The TEM values are, however, consistently larger than the TDS values. Two factors that could contribute to this difference are as follows. (i) The CO/Pt ratio of 0.7 used in the evaluation may be too large. However, at high dispersions the tendency is reported to be towards an even larger CO/Pt ratio around 0.9 (*33–36*), which would increase the difference between the TDS and TEM dispersion values. For larger particles a CO/Pt ratio of 0.5 has been reported (*35*). Thus the uncertainty in the CO/Pt ratio is not a likely cause of the TDS-TEM dispersion value difference. (ii) The TEM micrographs may contain particles

TABLE 1

Data for Fresh and Aged Catalysts Obtained by CO-TDS and TEM

Atmosphere	Temperature (°C)	Time (min)	Dispersion from TEM (no. of measured particles)	Mean (nm)	Range (nm)	Dispersion from CO-TDS
Fresh	—	—	n.m.[a]	≤1	—	0.36–0.50
H_2	700	60	n.m.[a]	≤1	—	0.40
Ar	700	60	n.m.[a]	≤1	—	0.43
O_2	500	60	n.m.[a]	≤1	—	0.43
O_2	600	60	0.16 (97)	6.0	2–10	0.10
O_2	700	10	0.20 (95)	4.5	1–9	0.08
O_2	700	60	0.15 (57)	8.9	2–11	0.06
CO	600	65	0.59 (estimated)	≈1.8	—	0.32
CO + NO	≈475	8	0.33 (107)	2.9	1–5	0.15
4% NO	300	60	0.13 (49)	6.9	2–12	0.08
4% NO	500	20	0.20 (75)	4.7	1–8	0.08
4% NO	500	10	0.12 (47)	7.5	5–12	0.06
0.1% NO	200	160	0.28 (57)	3.5	2–5	0.17
0.1% NO	300	120	0.20 (75)	4.9	2–8	0.15
0.1% NO	500	60	0.11 (111)	8.5	5–14	0.04

[a] nonmeasurable.

which are buried in closed pores of the support or have a major fraction of their surface area in contact with pore walls, so that they are not accessible for gas adsorption. This would result in too high dispersion values deduced from TEM. At present this appears to be the most likely reason for the observed difference.

Concerning the fresh samples, a reliable dispersion value cannot be obtained from TEM measurements, only a lower limit. Actually the continuum model represented by Eq. (1) fails for too small particle sizes (below 1 nm). In Fig. 8 the fresh samples are represented by a rectangle representing (vertically) the spread in initial CO-TDS dispersion values, and (horizontally) the regime where the dispersion values from TEM are not reliable (90–100%).

Due to the limited resolution in TEM there is still an open question whether the very initial losses of dispersion at high dispersion are due to real sintering (i.e., particle size growth) or to structural rearrangement of individual particles, causing a change in surface area and/or adsorption stoichiometry.

In summary, and recalling the reservations above, we note that the trends in the dispersion values deduced from CO-TDS and from TEM micrographs correlate well.

Particle Growth Mechanisms and Kinetics

Possible mechanisms for the sintering process, discussed in the literature, are (i) migration of single atoms or molecules between the clusters of atoms (particles) on the support, and (ii) motion of whole clusters over the support surface where they eventually collide and merge to a single, larger cluster.

In case (ii) of cluster migration they are supposed to move over the support, either as an unperturbed entity (primarily small clusters) or by random motion of atoms on the cluster surface, resulting in a net motion of the whole particle (somewhat like an amoeba motion). The "random walk" of these polyatomic clusters over the support is eventually accompanied by their collision and coalescence. The rate of migration normally depends sensitively on the size of the cluster and of the cluster–support interaction. Small clusters and/or weak interaction

with the support mean in general easier motion on the surface because of less/weaker bonds between metal particles and the support surface. A review of theoretical models for crystallite migration is found in Ref. (*19*).

The atomic/molecular migration mechanism (i) above may be either over the support or via an evaporation–condensation path. An important driving force for the particle growth at small cluster sizes is the lower stability of small clusters due to their larger surface energy, compared to larger ones. This size dependence, analogous to the size-dependent vapour pressure outside small spherical drops (the Kelvin equation), has been applied to emulsions of small particles in solution (*39*) as well as to catalyst particles on supports (*15*). In the latter case this size effect can be expressed as a higher vapour pressure of atoms/molecules around small particles or equivalently as a lower activation barrier, E, for emission of atoms/molecules from the cluster into the gas phase (E_{vap}) (evaporation), or alternatively onto the support (E_s). E_{vap} for a large particle is assumed to equal the sublimation energy H_{sub}, while E_s is generally expected to be lower than E_{vap}, since there is always some attractive interaction, E_{ms}, between the emitted atom/molecules and the support. Approximately one expects $E_s \approx E_{vap} - E_{ms}$. $E_{ms} > 0$ implies that the energetically most favoured interparticle transport is via atomic diffusion on the support. In the following we neglect the evaporation path.

Based on the Kelvin equation the dependence of E_s on the cluster radius, r, has been given by, for example, Wanke (*20*) as

$$E_s(r) = E_s(\infty) - \frac{\beta}{r}, \qquad (2)$$

where $E_s(\infty)$ is the activation energy for emission of an atom/molecule from a large cluster to the support ($E_s(\infty) = E_{vap} - E_{ms}$). In the derivation, Wanke assumed that the rate of emission from crystallites is independent of whether or not the system is at equilibrium. The value of β is dependent on cluster shape. For simplification we consider only hemispherical clusters. β then becomes $2\sigma V_m$ (see, for example, (*19*)), where σ is the metal–gas interfacial energy and V_m the molar volume of Pt.

Equation (2) states that the rate of emission of atoms/molecules increases rapidly for smaller particles since the rate varies as $\exp(-E_s(r)/RT)$. Estimates for a Pt dimer show that a factor of 2 reduction of $E_s(r)$ is quite realistic (*40*), as r becomes small. It is not our intention, however, to pursue a more quantitative analysis along these lines.

The simple analysis above serves as a background to discuss the experimental data. Generally the influence of a gas such as O_2 or NO on the sintering rate is likely to originate from the exponential dependence of the emission rate on the absolute value of $E_s(r)$ in Eq. (2). The added gas can increase the rate in two ways. First, the stability of large clusters may be lowered by a reduction of $E_s(\infty)$, i.e., by a reduction of E_{vap} or by an increase of E_{ms} or both. Second, the interfacial energy determining the value of β may change. Below we make some more specific comments along these lines, when the data for Ar, H_2, O_2, and NO are compared.

H_2, Ar. An estimation of the interaction between a metal and a support is obtained from the wetting experiments by Pilliar and Nutting (*41*). The work of adhesion for Ag, Cu, Au, Ni, and γ-Fe supported on α-alumina can be calculated from the relation between the work of adhesion and surface energies (for liquids). $W_a = \sigma_m + \sigma_s - \sigma_{ms}$, where σ_m, σ_s, and σ_{ms} are the surface energies for the metal, support, and metal–support interface, respectively. The values of W_a are ranging from 0.435 J/m^2 for Ag to 0.800 J/m^2 for γ-Fe, corresponding to metal–support bonding energies of about 20–40 kJ/mol, with an assumed surface density of 1×10^{19} atoms/m^2. (Note that these results are for α-alumina, while we are considering γ-alumina.)

The emission rate of atoms from particles can be estimated using the equation

$$\frac{dN}{dt} = \nu \exp(-E_s(r)/RT), \qquad (3)$$

where dN/dt is the emission of platinum atoms per site and second, ν is the so-called frequency factor, and $E_s(r)$ is the activation energy for emission onto the support from Eq. (2). Using the value of σ suggested by McLean and Hondros (*42*) (2.1 J/m^2), E_{vap} = 560 kJ/mol (*43*) and E_{ms} = 40 kJ/mol, we estimate the rate of Pt atom emission from a Pt particle with radius 0.5 nm to be $\approx 10^{-8}$ site^{-1} s^{-1} at 727°C. While in simple absolute rate theory ν is of the order of 10^{13} s^{-1}, we have in the estimate above used a high preexponential factor ν of 1×10^{15} s^{-1}. (This number was obtained using available vapour pressure data for Pt and assuming a sticking coefficient of one (*44*) for a Pt atom to stick on a Pt surface.) In spite of this large ν factor and a probable underestimate of the particle's energetic stability, it is still found to be highly stable. This consequently makes atomic migration improbable as a mechanism for sintering in H_2 up to 700°C, in line with the experimental findings.

The alternative mechanism of cluster migration should be favoured by weak metal–support interaction. Since no significant sintering was detected in H_2 at 600–700°C for 60 min, the rate of any cluster migration must also be very low. This is in accordance with the calculations made by Anderson (*40*), who used a model with random motion of atoms on the particle surface.

O_2. The considerably higher measured sintering rate in oxygen above 600°C than in hydrogen (or in noble gas) is in agreement with earlier reported results (*3, 7, 9, 10*). The very rapid initial sintering is followed by a quick stabilization as the particles grow larger. This could in principle be the result of either a cluster or an atomic/molecular migration process. Several observations support the latter mechanism.

We first note that according to Section 3 and Ref. (*45*) small Pt particles oxidize easily in oxygen at temperatures at or above 500°C. Oxidized Pt is less stable than Pt in metallic form. For example, it is well known that there is a significant weight loss of platinum in oxidizing atmospheres above 900°C, see, e.g., Refs. (*46, 47*).

The second factor to consider is the particle–support interaction. Wetting experiments with several metals on glass supports, reviewed by Geus (*48*) and Anderson (*40*), show a general trend of decreased wetting angle in oxidative atmospheres. Pask and Fulrath (*49*) observed the same behaviour for $Na_2Si_2O_5$-glass drops on platinum metal. When the metal is oxidized, it thus appears to interact more strongly with oxidic substrates. Another indication of a stronger oxidized metal–support interaction comes from measured surface energies in air in a study of grain-boundary grooving at the platinum/α-alumina interface by McLean and Hondros (*42*). Estimation of the work of adhesion gives $W_a \approx 1.8$ J/m^2. Assuming the same strength of interaction in the system of platinum/γ-alumina, the metal–support bonding energy should be about 90 kJ/mol.

Oxygen is thus expected to both reduce the cohesive energy (i.e., a reduction of E_{vap}) and increase the PtO_x–Al_2O_3 interaction (i.e., an increase of E_{ms}), causing a lower activation barrier for emission of migrating species onto the support.

In contrast, the larger particle–support interaction under oxidizing conditions will reduce the probability for cluster migration as whole entities compared to the metallic case.

We thus tentatively attribute the higher sintering rate in O_2, compared to inert or reducing atmospheres, to an increased transport rate between clusters. Likely candidates for the migrating species in O_2 are platinum oxide molecules (PtO or PtO_2).

A numerical estimate, for oxidized particles, is illustrative. From the Pt sublimation experiments in O_2 at 1200°C by Raub and Plate (*47*) one can estimate the PtO_x evaporation energy (x probably $\approx$ 2), using Eq. (3) with E_s replaced by E_{vap} and ν taken as above to be $\approx 10^{15}$ s^{-1}. From the measured

weight loss rate we obtain $E_{vap} \approx 480$ kJ/mol, to be compared to $E_{vap} = 560$ kJ/mol for metallic Pt in vacuum. This is probably a too large value, since we have not considered any readsorption in Eq. (3). An alternative estimate of E_{vap} is obtained as ΔH for the reaction $PtO_2(s) \rightarrow PtO_2(g)$. Combining the values of ΔH for the oxide formation $Pt(s) + O_2(g) \rightarrow PtO_2(s)$ ($\Delta H \approx -130$ kJ/mol (*50*)) and the reaction $Pt(s) + O_2(g) \rightarrow PtO_2(g)$ ($\Delta H \approx 180$ kJ/mol (*12, 21*)), the heat of evaporation of $PtO_2(s)$ becomes ≈ 310 kJ/mol. Even if we use the higher value of 480 kJ/mol and E_{ms} as 90 kJ/mol, we obtain (Eq. (3)) for a particle with $r = 0.5$ nm, an emission rate of order 10^{-2} s^{-1} site^{-1} at 700°C. This value demonstrates, in agreement with experiments, how the stability of an oxidized Pt particle is reduced compared to the metallic particle, primarily through a reduced cohesive energy.

NO. In NO the sintering rate is considerably larger than in O_2. It was noticeable even at such a low temperature as 200°C. The tendency for sintering is larger for preoxidized than for prereduced or only partially oxidized samples. The same qualitative explanation, as for O_2, can be used for the reduced stability and increased sintering rate in NO, i.e., it is primarily attributed to a reduced $E_s(\infty)$ for the oxidized Pt compared to metallic Pt. However, it remains to explain the surprising and dramatic difference in the sintering rate between O_2 and NO (note that the same saturation amount of oxygen was taken up in NO as in O_2 (Section 3)).

The paper by Handforth and Tilley (*51*) may elucidate this question. They measured the weight loss of a platinum gauze catalyst during ammonia oxidation and found a significant loss of platinum at much lower temperatures than during pure oxidizing conditions, which is similar to our observations. In the oxidation of ammonia, NO is formed via the reaction, $4NH_3 + 5O_2 \rightarrow 4NO + 6H_2O$, and NO is thus present during the process. Comparing our sintering results obtained with NO (for supported particles) and the ammonia oxidation results (for an unsupported catalyst), it appears that in both cases the stability of the (oxidized) platinum is strongly reduced by adsorbed NO (i.e., E_{vap} and thus $E_s(\infty)$ in Eq. (2) are lowered). The fact that NO really adsorbs on oxidized Pt was observed in Ref. (*31*) and in the present work.

It is possible to estimate the evaporation energy via the measured weight loss of platinum in the ammonia oxidation process and using Eq. (3). From the weight loss at 727°C (*51*), we obtain E_{vap} as 350 kJ/mol (no readsorption assumed). With this value for $E_s(\infty)$ in Eq. (3) and assuming the same interaction with the support as in the O_2 case, the emission rate of Pt atoms (Eq. (3)), for a particle with $r = 0.5$ nm, becomes $\approx 10^2$ site^{-1} s^{-1} at 500°C. The stability has thus decreased drastically in this NO-containing atmosphere, compared to in O_2, which is consistent with our experimental observations. A possible mechanism for this destabilization in NO is a dry etching-like effect, where the migrating species is a NO-containing Pt complex, with a lower activation barrier for emission from the oxidized Pt particle.

A more quantitative analysis must await numerical modeling of the sintering process along the lines discussed above. Such work is underway.

An additional qualitative comment is appropriate about the atom/molecule migration mechanism. The process could be limited either by atom/molecule emission to the support or by the diffusion rate on the support. We have assumed that the process is emission limited rather than diffusion limited. This assumption is partly based on the very fast initial sintering and the fact that no redispersion was observed at any temperature, as might be expected for a diffusion-limited transport on the support (*15*). Moreover, the activation energy for diffusion on the support, E_d, is likely to be low since it is related to the strength of interaction between metal atoms and the support and is commonly of the order $0.1\ E_{ms}$ (*14*).

5. CONCLUSIONS

Highly dispersed Pt clusters (diameters ≈ 1 nm) on γ-alumina are found to be stable towards sintering in reducing (H_2) and inert atmospheres up to 700°C. In contrast, oxidizing atmospheres of O_2 or NO, accelerate the sintering rate. In O_2 noticeable sintering is observed at 600°C. The effect of NO is more dramatic in that significant sintering is observed down to 200°C. The decreased stability in O_2 and NO, compared to H_2 or Ar, is attributed to a reduction of the cohesive energy of oxidized as compared to metallic Pt, with possible additional influence from differences in the particle–support interaction strength. NO adsorbed on oxidized Pt particles obviously enhances this effect further.

The rapid stabilization towards sintering as the clusters grow larger is attributed to the size-dependent surface energy, which makes the smallest clusters quite unstable in oxidizing atmospheres. The rate limiting mechanism of material transport is probably emission of $Pt–O_x$ complexes from the oxidized clusters to the support. Cluster migration and diffusion-limited transport appear to be less likely mechanisms; for the present conditions of particle size, temperature, support, and gaseous environment, cluster migration is estimated to be too slow to play a role, while diffusion on the support is too rapid to be rate limiting.

Comparing Pt dispersion values measured by CO-TDS and TEM, respectively, a good correlation is observed, but the quantification uncertainties are fairly large. The two methods are complementary; CO-TDS is most sensitive at the highest dispersion, where the uncertainty is largest with TEM due to small particle sizes.

ACKNOWLEDGMENTS

The authors are grateful to the National Swedish Board for Technical Development for financial support of the projects (Grants 89-5405, 87-01446P, 90-1545, and 89-01096P). We are also grateful to Svenska Emissionsteknik AB for preparing the samples.

REFERENCES

1. Chu, Y. F., and Ruckenstein, E., *J. Catal.* **55,** 281 (1978).
2. Harris, P. J. F., Boyes, E. D., and Cairns, J. A., *J. Catal.* **82,** 127 (1983).
3. Beck, D. D., and Carr, C. J., *J. Catal.* **110,** 285 (1988).
4. Harris, P. J. F., *J. Catal.* **97,** 527 (1986).
5. Fiedorow, R. M. J., and Wanke, S. E., *J. Catal.* **43,** 34 (1976).
6. Glassl, H., Kramer, R., and Hayek, K., *J. Catal.* **68,** 388 (1981).
7. White, D., Baird, T., Fryer, J. R., Freeman, L. A., Smith, D. J., and Day, M., *J. Catal.* **81,** 119 (1983).
8. Sushumna, I., and Ruckenstein, E., *J. Catal.* **109,** 433 (1988).
9. Guo, I., Yu, T. T., and Wanke, S. E., *in* "Catalysis 1987" (J. W. Ward, Ed.), Studies in Surface Science and Catalysis, Vol. 38, p. 21. Elsevier, Amsterdam, 1988.
10. Fiedorow, R. M. J., Chahar, B. S., and Wanke, S. E., *J. Catal.* **51,** 193 (1978).
11. Baker, R. T. K., Thomas, C., and Thomas, R. B., *J. Catal.* **38,** 510 (1975).
12. Rickard, J. M., Genovese, L., Moata, A., and Nitsche, S., *J. Catal.* **121,** 141 (1990).
13. Freel, J., *J. Catal.* **25,** 139 (1972).
14. Wynblatt, P., and Gjostein, N. A., *Prog. Solid State Chem.* **9,** 21 (1975).
15. Flynn, P. C., and Wanke, S. E., *J. Catal.* **34,** 390, 400 (1974).
16. Flynn, P. C., and Wanke, S. E., *J. Catal.* **37,** 432 (1975).
17. Ruckenstein, E., and Pulvermacher, B., *J. Catal.* **29,** 224 (1973).
18. Ruckenstein, E., and Dadyburjor, D. B., *J. Catal.* **48,** 73 (1977).
19. Lee, H. H., and Ruckenstein, E., *Catal. Rev. -Sci. Eng.* **25,** 475 (1983).
20. Wanke, S. E., *in* "Sintering and Catalysis," *Mater. Sci. Res.* **10,** 107 (1975).
21. Wynblatt, P., and Ahn T-M., *in* "Sintering and Catalysis," *Mater. Sci. Res.* **10,** 83 (1975).
22. Önal, I., *in* "Catalyst Deactivation 1991" (C. H. Bartholomew and J. B. Butt, Eds.), Studies in Surface Science and Catalysis, Vol. 68, p. 621. Elsevier, Amsterdam, (1991).
23. Stenbom, B., Smedler, G., Nilsson, P. H., Lundgren, S., and Wirmark, G., "SAE Technical Paper Series," No. 900273. SAE, New York, 1990.
24. Lööf, P., Kasemo, B., and Keck, K.-E., *J. Catal.* **118,** 339 (1989).
25. Kasemo, B., *Rev. Sci. Instrum.* **50,** 1602 (1979).
26. Rice, S. B., and Treacy, M. M. J., *Mater. Res. Soc. Symp. Proc.* **115,** 15 (1988).
27. Flynn, P. C., Wanke, S. E., and Turner, P. S., *J. Catal.* **33,** 233 (1974).

28. Treacy, M. M. J., and Howie, A., *J. Catal.* **63,** 265 (1980).
29. Foger, K., and Anderson, J. R., *Appl. Surf.Sci.* **2,** 335 (1979).
30. Herz, R. K., and McCready, D. F., *J. Catal.* **81,** 358 (1983).
31. Lööf, P., Kasemo, B., Anderson, S., and Frestad, A., *J. Catal.* **130,** 181 (1991).
32. Kasemo, B., and Törnqvist, E., *Phys. Rev. Lett.* **44,** 1555 (1980), and the references therein.
33. Yao, H. C., Sieg, M., and Plummer, H. K., Jr., *J. Catal.* **59,** 365 (1979).
34. Wilson, G. R., and Hall, W. K., *J. Catal.* **17,** 190 (1970).
35. Dorling, T. A., and Moss, R. L., *J. Catal.* **7,** 378 (1967).
36. Freel, J., *J. Catal.* **25,** 149 (1972).
37. McCabe, R. W., and Schmidt, L. D., *Surf. Sci.* **66,** 101 (1977).
38. Rothschild, W. G., and Yao, H. C., *J. Chem. Phys.* **74,** 4186 (1981).
39. Wagner, C., *Z. Elektrochem.* **65,** 581 (1961).
40. Anderson, J. R. "Structure of Metallic Catalysts," Chap. 5. Academic Press, London, 1975.
41. Pilliar, R. M., and Nutting, J., *Philos. Mag.* **16,** 181 (1967).
42. McLean, M., and Hondros, E. D., *J. Mater. Sci.* **6,** 19 (1971).
43. Knacke, O., Kubaschewski, O., and Hesselmann, K., "Thermochemical Properties of Inorganic Substances II," second ed. Springer-Verlag, Berlin, 1991.
44. Langmuir, I., *Phys. Rev.* **2,** 329 (1913).
45. Lööf, P., Kasemo, B., Björnkvist, L., Andersson, S., and Frestad, A., *in* "Catalysis and Automotive Pollution Control II" (A. Crucq, Ed.), Studies in Surface Science and Catalysis, Vol. 71, p. 253. Elsevier, Amsterdam, 1991.
46. Schäfer, H., and Tebben, A., *Z. Anorg. Allg. Chem.* **304,** 317 (1960).
47. Raub, E., and Plate, W., *Z. Metallkd.* **48,** 529 (1957).
48. Geus, J. W. *in* "Chemisorption and Reactions on Metallic Films" (J. R. Anderson, Ed.), Chap. 3. Academic Press, London, 1971.
49. Pask, J. A., and Fulrath, R. M., *J. Am. Ceram. Soc.* **45,** 592 (1962).
50. Samsonov, G. V., "The Oxide Handbook," p. 42. IFI/Plenum, New York, 1973.
51. Handforth, S. L., and Tilley, J. N., *Ind. Eng. Chem.* **26,** 1287 (1934).